Mon. Not. R. Astron. Soc. **377,** 1195–1205 (2007) doi:10.1111/j.1365-2966.2007.11670.x

The nature of the Wolf–Rayet galaxy Mrk 209 from photoionization models

Enrique Pérez-Montero[1,2★†] and Ángeles I. Díaz[2‡]

[1]*Institute d'Astrophysique de Toulouse-Tarbes, Observatoire Midi-Pyrénées, 14 avenue Edouard Belin, 31400 Toulouse, France*
[2]*Departamento de Física Teórica, C-XI, Universidad Autónoma de Madrid, 28049 Madrid, Spain*

Accepted 2007 February 23. Received 2007 February 2; in original form 2006 November 14

ABSTRACT

We present a detailed photoionization model of the brightest knot of star formation in the blue compact dwarf galaxy Mrk 209. The model reproduces the intensities of main lines emitted by the ionized gas, resulting in a very good agreement between observed and predicted line temperatures and chemical abundances of the observed ionic species.

The model has been calculated using the spectral energy distribution of a massive cluster of recent formation as the ionizing source. The features of Wolf–Rayet (WR) stars observed in the spectrum of the object, along with its ionizing properties, lead to different solutions for the ages and characteristics of the ionizing stellar populations. The found solutions are compatible with either a composite population of two ionizing clusters or a continuous star formation. In the first case, a young cluster, with an age less than 3 Myr, would be responsible for most of the ionization properties while an older cluster, with either 3.2 or 4.2 Myr, would be responsible for the emission of the observed WR features in the spectrum of the knot. In the second case, the duration of the star formation episode is found to be 3.6 Myr.

The addition of a certain amount of dust was required in order to reproduce correctly the measured electron temperatures. This dust implies a gas/dust ratio of 6.13×10^{-3}, identical to that in the Milky Way, and a fraction of absorbed photons of $f = 0.58$. The taking into account the dust grain physics combined with a thick-shell geometry solves the problem of the heating in this object and allows the fitting of the auroral lines, the line temperatures and the ionization structure of the nebula with a negligible presence of temperature fluctuations, in agreement with the most recent results found for this type of objects from the measurement of the Balmer jump temperature.

An analysis of the ionization structure of the gas as well as the calculation of the main ionization correction factors for the unseen ionic stages is presented.

Key words: ISM: abundances – H II regions – galaxies: starburst.

1 INTRODUCTION

Blue compact dwarf (BCD) galaxies are objects whose spectra, as in the case of H II regions, are dominated by emission lines from the gas ionized by very recent episodes of star formation (Sargent & Searle 1970). Many intermediate redshift objects have properties similar to the BCD in the Local Universe and it is possible that they were common in the past and they have evolved to other kind of objects. Therefore, the study of the star-forming history in BCDs is of great importance.

In general, BCDs are characterized by their compact aspect, very low metallicities, gas richness and blue colours (Kunth & Östlin 2000). These properties have made of them good candidates to host their first episodes of star formation. Nevertheless, recently, the detection in most of them of low surface-brightness elliptical haloes, or the presence of stars belonging to older populations, have caused this interpretation to be reconsidered. Nowadays, only few candidates remain controversial.

There are several works in the literature whose main aim is to study the weight of these older stellar populations in BCDs and, hence, to find out the actual age and evolutionary status of these objects. Among these studies, in the sample of local objects, observations with enough spatial resolution to provide photometry of the individual stars have allowed, by means of colour–magnitude diagrams, to date some of the bursts (e.g. VII Zw403 by

★E-mail: enrique.perez@ast.obs-mip.fr
†Post-Doc fellow of Ministerio de Educación y Ciencia, Spain.
‡On sabbatical leave at IoA, Cambridge.

Schulte-Ladbeck, Crone & Hopp 1998; IZw18 by Aloisi & Leitherer 2000). In all these works evidences for stellar populations older than 500 Myr have been found. Besides, old stellar low surface brightness components have been detected in these local objects by studying the radial light distribution in the optical (e.g. Gil de Paz, Madore & Pevunova 2003) and the near-infrared (near-IR) (e.g. Noeske et al. 2005).

For more distant galaxies, the study of the stellar population is limited to the interpretation of the integrated spectrophotometric properties by means of empirical and evolutionary population synthesis techniques. The results from this kind of works (e.g. Raimann et al. 2000) show that most blue compact dwarves are age-composite stellar systems, with discontinuous star-forming histories.

Nevertheless, there is still a lack of spatially resolved studies of the properties of the ionizing stellar populations and the ionized surrounding gas in the different knots of star formation. This work is usually approached by means of photoionization models, trying to reproduce the measured fluxes and equivalent widths (EWs) of the lines emitted by the ionized gas, under different assumptions about its geometry, metal content and ionizing incident radiation. Several improvements have been produced that increase our confidence in the results from this kind of models: inclusion of blanketing effects in O and Wolf–Rayet (WR) expanding stellar atmosphere models (Pauldrach, Hoffmann & Lennon 2001; Smith, Norris & Crowther 2002) and recent computation of non-local thermodynamic equilibrium (NLTE) blanketed plane-parallel models (Lanz & Hubeny 2003). Yet, model computed evolutionary sequences show important disagreements with observations. Among others, the [O III]/Hβ versus [O II]/Hβ and [O III]/Hβ versus [O I]/Hβ relations are not well reproduced by evolutionary model sequences in the sense that predicted collisionally excited lines result too weak compared to observations, which would require additional heating mechanisms or the presence of chemical inhomogeneities (Stasińska & Izotov 2003).

These facts seem to point out to a still incomplete description of the ionization structure of the emitting nebulae which would improve with the determination of more than one line electron temperature. This has been attempted recently by several authors (e.g. Garnett 1989; Pérez-Montero & Díaz 2003, hereafter PMD03; Hägele et al. 2006) by enlarging the spectral sampling to include the lines of [O II] at $\lambda\lambda$ 7319, 30 Å and [S III] at $\lambda\lambda$ 9069, 9532 Å. The far-red [S III] emission lines can provide better estimates of the ionization parameter of the gas, via the [S III]/[S II] quotient (Díaz et al. 1991), and the equivalent effective temperature of the ionizing clusters, via the η parameter (Vílchez & Pagel 1988), than the widely used strong optical lines of oxygen, mainly due to their lower dependence on other quantities, such as age or metallicity. These parameters are key factors to provide adequate input constraints for photoionization models.

Although the detection and analysis of the near-IR emission lines is hampered by the strong and variable absorption features of the Earth's atmosphere, a thorough atmospheric extinction correction and a good spectral resolution aid to remove the sky background providing a good level of confidence in the measurement of the far red [S III] lines. The number of H II galaxies observed both in the optical and the far-red spectral range, up to 1 μm, is still scarce but it is steadily increasing.

In this work, we apply a detailed photoionization model to the brightest knot of the BCD Mrk 209, for which both wide range spectroscopic observations and photometric data exist.

In the next section we describe the properties of Mrk 209 as given in the literature, focusing on the main burst of star formation, measuring their photometric properties and the gas physical conditions. In Section 3 we describe the photoionization model we have used with the inclusion of the input stellar ionizing population and the effects of dust. Section 4 presents and discusses the model results in comparison with observations. Finally, the conclusions of this work are presented in Section 5.

2 PROPERTIES OF THE OBJECT

Mrk 209, also known as IZw36 and UGCA 281, is a BCD galaxy that has been extensively studied. The work by Viallefond & Thuan (1983) revealed a core–halo structure of the diffuse neutral gas, with the star-forming regions located near the core, but slightly shifted with respect to the peak in H I column density. They measured its virial mass which is about six times that in H I, which could imply a large contribution of dark matter. Loose & Thuan (1986) discovered an extended, elliptical background sheet underlying the compact, actively star-forming core and they classified this galaxy as *iE*, corresponding to blue compact dwarves with an irregular burst of star formation in its core, surrounded by regular elliptical isophotes.

Although Fanelli, O'Connell & Thuan (1988), from an *IUE* UV spectral study, pointed to Mrk 209 being a young galaxy undergoing its first episode of star formation, later works have ruled out this conjecture. The red colours observed by Deharveng et al. (1994) and by Papaderos et al. (1996) require the presence of old stellar populations in the elliptical host galaxy. Schulte-Ladbeck et al. (2001) were able, by means of *Hubble Space Telescope* observations with FOC in the optical and NICMOS in the near-IR, to build a colour–magnitude diagram identifying individual stars of the red giant branch, some of them with ages between 1 and 2 Gyr. These authors claim for an almost-continuous star formation history for this galaxy with inactive periods never longer than 100 Myr.

Gil de Paz et al. (2003, hereafter GMP03) have produced photometric observations in Hα and the *B* and *R* bands. They find that the Hα emission peaks at a region towards the west of the galaxy, accompanied by two weaker star-forming regions towards the east. The weakest of these regions lacks near-IR emission (Noeske et al. 2005) implying that the dominant population is still very young.

Regarding the brightest knot of star formation, Deharveng et al. (1994) showed that their young stars have an age less than 12 Myr. Later evolutionary synthesis models by Mas-Hesse & Kunth (1999) have lowered this upper limit further to only ≈2.7 Myr. Besides, Izotov, Thuan & Lipovetsky (1997, hereafter ITL97) and Schaerer, Contini & Pindao (1999) discovered WR features in this knot.

Spectrophotometric observations in the range between 3000 and 7800 Å from ITL97 and between 7000 and 9800 Å (PMD03) exist for this burst. The slit width used in both works is identical and the agreement of the relative fluxes in the coincident spectral range is good; therefore, we can be confident about the spatial coincidence of both sets of observations. The intensities and EWs of the observed WR features were measured by Guseva, Izotov & Thuan (2000, hereafter G00).

We have collected the main photometric and spectroscopic properties of the brightest knot of star formation in Table 1. Regarding the spectroscopic data, WR feature intensities and EWs (G00) refer to a slit width of 2 arcsec, while the emission-line fluxes, Hβ EW and reddening constant C(Hβ) (ITL97; PMD03) refer to a slit width of 1.5 arcsec. Besides, we have compiled *ISO* observations of this object (Nollemberg, Garnett & Dinerstein 2002) that account for line intensities of 4.05 μm Brα, 10.5 μm [S IV] and 18.7 μm [S III] in the mid-IR. Nevertheless, the apertures used for these observations are much larger that those used in the optical and the near-IR, and

Table 1. Properties of the main burst of star formation in Mrk 209.

Distance (Mpc)	6.6 ± 1.1
$F(\mathrm{H}\alpha)^a$	14.97 ± 0.01
Z^b	0.0036
$C(\mathrm{H}\beta)$	0.06
B (mag)^c	16.58 ± 0.13
$B - R$ (mag)	0.28 ± 0.18
EW(Hβ) (Å)	206
EW(4650 Å) (Å)	5.01 ± 0.10
log L(4650 Å)^d	37.35 ± 0.13
EW(5808 Å) (Å)	1.74 ± 0.15
log L(5808 Å)^e	36.62 ± 0.16

^{a}In units of 10^{-13} erg s^{-1} cm^{-2}. ^{b}In mass, scaled to the oxygen solar abundance from Allende-Prieto (2001). ^{c}Not corrected for reddening. ^{d}In units of erg s^{-1}.

Table 2. Emission-line intensities, relative to Hβ = 100, with their corresponding errors, observed and the predicted by our model and the model in PMD03.

Emission line	Observed	This model	PMD03
3727 Å [O II]^a	71.9 ± 0.2	69.4	68.7
3868 Å [Ne III]^a	45.7 ± 0.1	46.0	–
4072 Å [S II]^a	1.2 ± 0.1	1.2	–
4363 Å [O III]^a	12.7 ± 0.1	12.4	9.6
4658 Å [Fe III]^a	0.3 ± 0.1	0.4	–
4959 Å [O III]^a	196.0 ± 0.3	190.1	200.8
5007 Å [O III]^a	554.3 ± 0.8	574.2	604.4
6584 Å [N II]^b	3.6 ± 0.1	3.6	–
6725 Å [S II]^b	10.6 ± 0.4	10.2	6.8
6312 Å [S III]^b	1.9 ± 0.1	1.9	1.1
7137 Å [Ar III]^b	5.5 ± 0.1	5.6	–
7325 Å [O II]^b	1.7 ± 0.2	2.6	2.4
9069 Å [S III]^b	12.2 ± 1.2	12.1	8.7
10.5 μm [S IV]^c	42.6 ± 7.6	16.5	–
18.7 μm [S III]^c	17.4 ± 4.5	9.7	–

^{a}From Izotov et al. (1997); ^{b}from Pérez-Montero & Díaz (2003); ^{c}from Nollenberg et al. (2002).

although this is not expected to affect the fluxes of the lines of the ions of high excitation it could affect the hydrogen recombination line to some extent.

Luminosities have been derived assuming a distance of 6.6 ± 1.1 Mpc (Schulte-Ladbeck et al. 2001). The quoted errors for luminosities include the uncertainty in the distance to the galaxy. Regarding the photometric data, we have selected the area of the Hα image from GMP03 containing the same flux as in G00 corrected for aperture, and we have remeasured the B and R magnitudes in the corresponding images. The selected region has a mean radius of 72 ± 18 pc. The reddening corrected emission-line intensities, relative to Hβ = 100, are given in Table 2.

Using these emission-line data we have recalculated the electron temperatures and density, and the ionic chemical abundances. We have used the same algorithm described in PMD03: the five-level statistical equilibrium model in the TEMDEN and IONIC tasks of the NEBULAR package in STSDAS (of the program IRAF), based on the FIVEL program developed by De Robertis, Dufour & Hunt (1987) and improved by Shaw & Dufour (1995). We have used the transition probabilities and collision strengths included in the photoionization code CLOUDY (version 96.0; Ferland et al. 1998), except in the case of O^+ for which we have used the transition probabilities from Zeippen (1982) and the collision strengths from Pradham (1976), which offer more reliable results for nebular diagnostics (Wang et al. 2004) for this species.

Table 3. Properties of the modelled H II region.

	Observed	This model
EW(Hβ)	206 Å	210 Å
log Q(H)^a	51.75 ± 0.13	51.96^b
log U	-2.3 ± 0.1	−2.22
Filling factor		0.077
Inner radius		30 pc
Strömgren radius	72 ± 18 pc	48 pc
Absorption factor f		0.58
Dust-to-gas ratio		6.13×10^{-3}
$C(\mathrm{H}\beta)$	0.06	0.19

^{a}In photons s^{-1}. ^{b}Not absorbed by dust.

3 MODEL DESCRIPTION

The model here described simulates the properties of the ionized gas and the stellar ionizing population of the brightest knot of star formation in Mrk 209. It has been calculated using the photoionization code CLOUDY (Version 96.0, Ferland et al. 1998). This model is characterized by a set of input parameters including the ionizing continuum, the nebular geometry, the gas density and chemical abundances. The main properties of the best-fitting model are summarized in Table 3.

3.1 The ionizing stellar population

The WR phase in the evolution of massive stars is a short and transient stage, and therefore the presence of WR features in the spectrum of a star-forming region allows a dating of the ionizing stellar population. The emission features usually observed consist of two broad bumps. The first, usually called as *blue* is at 4650 Å and is a blend of the N V λ 4605, 4620 Å, N III λ 4634, 4640 Å, C III/C IV λ 4650, 4658 Å and He II λ 4686 Å broad WR lines. These are emitted mainly by WN and early WC stars. Besides, early WN stars emit broad emission features of C IV at λ 5808 Å, known as the *red* bump. Although the number of WR stars is expected to be much lower in relation to the number of O stars at low metallicites, they have been detected in the spectra of some BCDs, including Mrk 209 (ITL97, Schaerer et al. 1999) implying the presence of stars in the burst with an age between 1 and 5 Myr, that is the age of the WR stars.

We have calculated the spectral energy distributions of ionizing star clusters in this range of ages using evolutionary synthesis techniques (STARBURST 99; Leitherer et al. 1999) with the inclusion of the implementation by Smith et al. (2002) using the model atmospheres from Pauldrach et al. (2001) and Hillier & Miller (1998) for O and WR stars, respectively, which include the effects of blanketing. The used initial mass function is a Salpeter's one, with masses between 0.8 and 120 $M_\odot$. The supernova cut-off mass has been set to 8 $M_\odot$ and the black hole cut-off mass is at 120 $M_\odot$. We have considered a metallicity for the models equal to 0.004, 1/20 $Z_\odot$, which is very close to the metallicity derived for this object, equal to 0.0036. We have considered models with both standard and high mass-loss to explore which models fit better the observed properties of the object.

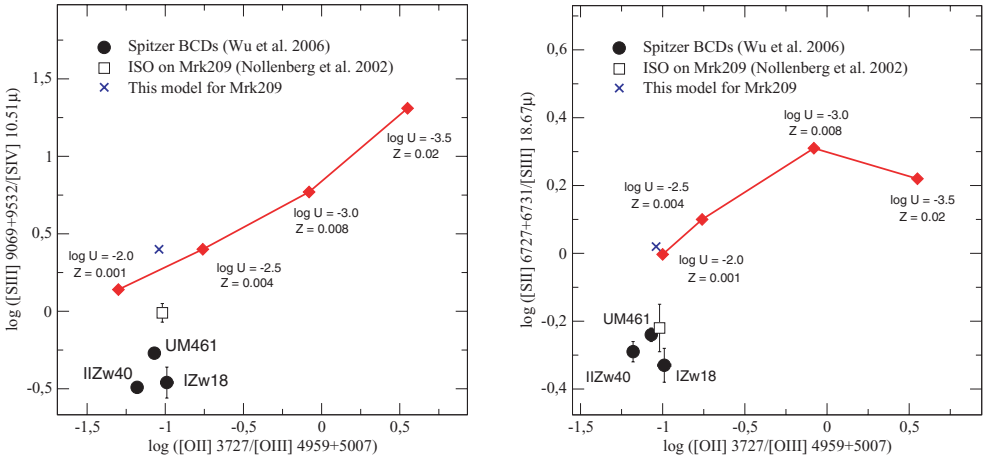

Figure 1. Diagnostic diagrams of the quotients of [S IV] 10.51 μm/[S III] (9069 + 9532 Å), in the left-hand panel and of [S III] 18.67 μm/[S II] (6717 + 6731 Å), in the right-hand panel, versus the quotient of [O II] 3727 Å/[O III] (4959 + 5007 Å), for a sample of BCD galaxies observed both in the near and the mid-IR and for a sequence of models covering the physical conditions of ionized gaseous nebulae. All model sequences, including the model presented here, fail to predict correctly the intensities of the sulphur emission lines in the mid-IR.

3.2 Nebular geometry

One of the input parameters of the models is the inner radius of the ionized region. In the most successful model, which is the one presented here, the ionization front is located at a distance of 30 pc of the ionizing source. Since the thickness of the H II region reaches approximately 18 pc, the resulting nebular geometry is a thick shell. The total radius, therefore, is not far from that measured on the Hα image around the brightest knot, 72 ± 18 pc, encompassing the same flux measured in the slit and corrected for aperture effects by G00. This geometry, along with a filling factor of 0.077 leads to a value of the spherical ionization parameter log $U = -2.22$, coincident with the value -2.3 ± 0.1 calculated by PMD03. This model considers a constant density of 190 particles per cm^3, which is the value obtained from the quotient of fluxes of the lines of [S II].

3.3 Dust content

We have added a certain amount of dust in order to fit correctly the measured electron temperatures. The presence of solid grains within the ionized gas have some consequences on the physical conditions of the nebula that should not be neglected, including the depletion of metals in gaseous form on to grains or the absorption of energetic radiation. The heating of the dust can affect, hence, the equilibrium between the cooling and heating of the gas and, thus, the electron temperature inside the nebula. The command PGRAINS, included in the last version of CLOUDY, implements the presence of dust grains as described in van Hoof et al. (2004). This command resolves the grain size distribution into several bins and treats each bin with its corresponding temperature, potential and drift velocity, which depend on the diameter of each grain. We have assumed the default grain properties of CLOUDY 96, which has, essentially, the properties of the interstellar medium and follows a MRN (Mathis, Rumpl & Norsieck 1977) grains size distribution.

4 RESULTS AND DISCUSSION

We find that the model that better fits the observed line intensities, the derived ionic abundances and the other observational properties of this knot is well represented by an instantaneous burst of 1.0 Myr. The inclusion of another burst in the WR phase in order to explain the observed features does not affect the ionization structure of the nebula and the obtained results. This result is equivalent assuming a constant star formation rate for the ionizing burst in such a way that its present age was that in the WR phase. The predicted emission-line intensities relative to Hβ = 100 are presented in column 3 of Table 2 and can be compared with the observed ones listed in column 2, and with those predicted by the best-fitting model in PMD03.

We can see all the relevant emission lines are better fitted by the present model than by that presented in PMD03 in which the ionizing radiation was represented by the CoStar atmosphere of a single massive star and a plane-parallel geometry was assumed. Using that model, it was not possible to reproduce the observed T([O III]) due to the underestimate of the auroral line at 4363 Å. On the other hand, an incorrect simultaneous fitting of the strong lines of [O II], [O III], [S II] and [S III] caused an overestimate of the η' parameter, defined as

$$\eta' = \frac{\mathrm{I([O\,II]3727)/I([O\,III](4959+5007))}}{\mathrm{I([S\,II](6717+6731)/I([S\,III](9069+9532))}}$$

(Vílchez & Pagel 1988), which is indicative of the temperature of the radiation field. In the present model, by means of including a more reallistic ionizing spectral energy distribution, derived from the evolutionary synthesis of the ionizing cluster, dust physics and an appropriate geometry, we have been able to reproduce adequately the main emission-line intensities. Nevertheless, the model is not able to reproduce the mid-IR lines observed with ISO, obtaining values for both [S III] 18.7μm and [S IV] 10.5 μm lower than observed by 60 and 40 per cent, respectively. This illustrates the problem that photoionization models have in general to correctly reproduce the intensities of sulphur emission lines in this spectral range. In Fig. 1 we represent the quotients of the lines of [S IV] 10.5 μm/[S III] (9069 + 9532 Å), in the left-hand panel and of [S III] 18.7 μm/[S II] (6717 + 6731 Å), in the right-hand panel, versus the quotient of [O II] 3727 Å/[O III] (4959 + 5007 Å), for a sample of BCDs observed both in the mid-IR with *Spitzer* (IZw18, UM461 and IIZw40; (Wu et al. 2006)) and *ISO* (Mrk 209; Nollenberg et al. 2002) and the near-IR: UM461, IIZw40 and Mrk 209 (PMD03), IZw18 (Garnett 1989). The comparison with the model presented here and a sequence of CLOUDY models simulating nebulae of different physical conditions

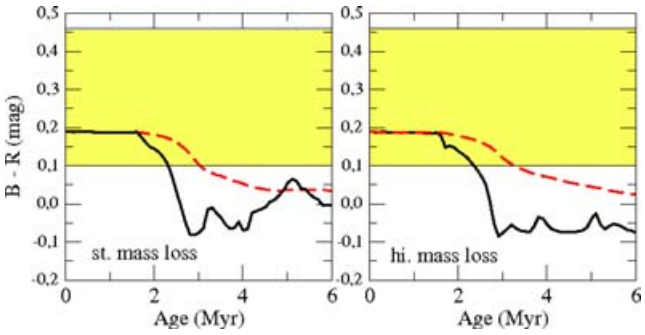

Figure 2. The colour index $B-R$ predicted by evolutionary synthesis models for both standard and high mass-loss stellar evolution and for instantaneous (thick solid line) and continuous (dashed line) star formation rates. The bands represent the values measured in the brightest star-forming region in the photometric images.

(ionization parameter between 3×10^{-4} and 1×10^{-2} and metallicity between 1/20 and 1 $Z_{\odot}$) ionized by a very young cluster shows serious discrepancies with observations for the prediction of the fluxes of the sulphur lines at mid-IR.

4.1 Inner extinction

The inclusion of grain physics helps to reproduce the intensity of the [O III] at 4363 Å, which depends exponentially on electron temperature. This shows the relevance of the presence of dust in the nebula. The required amount of dust implies a dust-to-mass ratio equal to 6.13×10^{-3}, almost identical to that found for the Milky Way (Spitzer 1978). This amount of dust for the column density predicted by the model, implies a visual extinction of $A_{\rm V} = 0.39$ mag and would correspond to a logarithmic extinction at Hβ of 0.19. This is higher than derived from the Balmer decrement [C(Hβ = 0.00; ITL97), C(Hβ = 0.06; G00)], but consistent with what is expected when comparing the computed ionizing star cluster colour index ($B-R$) with the observed one. Assuming that the presence of any older stellar population has not a relevant weight for this emitting knot, we can calculate the effect of the extinction by the dust present in the nebula on the synthesized ($B-R$) colour. The predicted ($B-R$) colour index for the synthesized clusters as function of age is shown in Fig. 2. The average colour predicted by instantaneous bursts of star formation for the ages between 2 and 5 Myr assumed in our models is around -0.05. This is bluer than the colour index measured for the knot which is $B-R = 0.28 \pm 0.18$. However, according to our model, the predicted colour should be reddened by 0.24 mag for the required amount of dust, which would make it consistent with observations.

The effect of dust has to be considered when calculating the number of ionizing photons reaching the gas. In fact, only a fraction f of the number of ionizing photons emitted by the cluster will ionize the gas

$$Q(\mathrm{H}) = f\,Q_0(\mathrm{H})$$

For the amount of dust required to reproduce the emission-line intensities in our model, we obtain $f \approx 0.58$.

4.2 Ionizing stellar populations

The comparison between the observed intensities and EWs of the blue and red bumps and those predicted by the models is shown in Fig. 3. The light-coloured bands represent the intensities and the EWs of the WR features with their corresponding errors as measured by G00 inside the slit. The dark-coloured bands represent the same quantities corrected for different effects: in the case of EWs, for the contribution of the nebular continuum, that is 20 per cent of the ionizing continuum at the wavelength of the blue bump and 25 per cent at that of the red bump, as predicted by our model; for

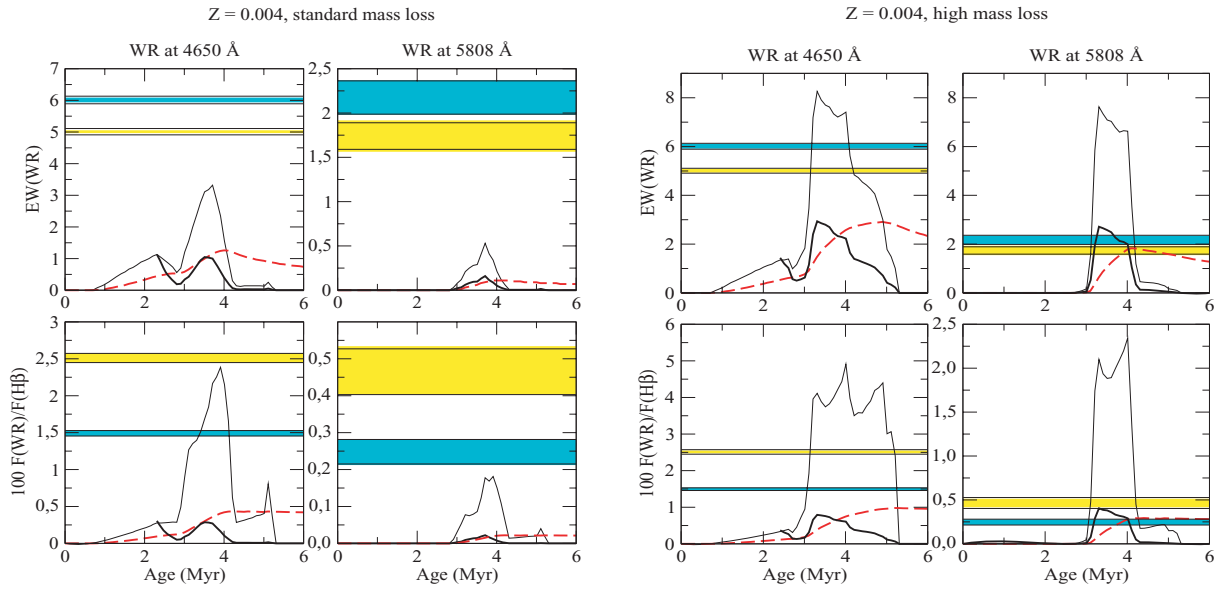

Figure 3. Comparison between the intensities and EWs of WR red and blue bumps observed in Mrk 209 and those predicted by the models. In the left-hand panels, models with standard mass-loss and in the right-hand panels, with high mass-loss. Both have been calculated for a metallicity $Z = 0.004$. The clear bands stand for the observed values with their errors as published in G00. The dark bands stand for the observed values once corrected for nebular continuum, in the case of EW and the fraction of absorbed ionizing photons, in the case of relative intensities. Models for an instantaneous burst are plotted as a solid thin black line. Models for a continuous star formation are plotted with a dashed line. Finally, the solid thick line represents models of a composite population with an instantaneous burst with an age of 1 Myr, resulting in the expected EW(Hβ).

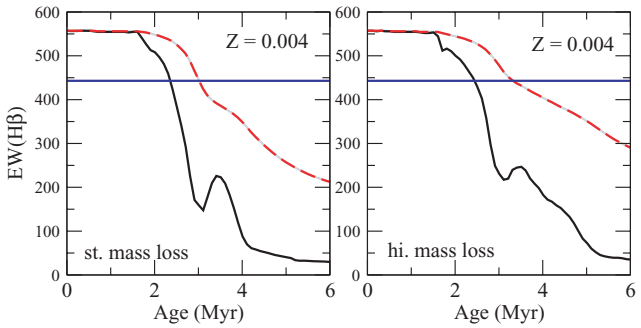

Figure 4. Prediction of the models for the EW of Hβ for both standard and high mass-loss and for instantaneous (thick solid line) and continuous (dashed line) star formation rate. The horizontal line represents the observed EW(Hβ, once subtracted the nebular continuum and corrected for the amount of absorbed ionizing photons as predicted by our model.

the relative fluxes, the correction is due to the absorption of ionizing photons by dust, affecting the intensity of Hβ. Regarding models the solid thin line represents the predictions by a model with a unique instantaneous burst whose age is that shown by the *X*-axes, and the dashed line the prediction for a burst with continuous star formation. Agreement between the observed and predicted relative intensities and EWs of the WR features is seen only for the models with a high mass-loss rate and for an instantaneous burst of approximately 3.0 Myr. Nevertheless, the slope of the models is very steep at this age, corresponding to the appearance of WR stars. In fact the WR phase provides a narrow age interval in which a solution is possible. The same is found in other works which use similar techniques ultimately based on stellar evolution models (e.g. González Delgado & Pérez 2000, on NGC 604). Two solutions are almost in all cases bound to exist: one at the age at which stars start to appear and another one when they start to decline, the precise values of these ages depending on the specific stellar evolution model predictions. The results of our models point to the earlier of these ages, that is, the beginning of the WR phase, as the most probable age for the cluster.

Another important constraint to the model is the EW of Hβ, which is an estimator of the age of the ionizing burst.[1] Again the value of 206 Å reported by G00 has to be corrected for the contribution of nebular continuum and absorption of ionizing photons by dust. These effects increase the value of EW(Hβ) produced by the cluster to 443 Å. This value is much higher than predicted by STARBURST 99 models for a cluster of 3.0 Myr and high mass-loss rate as it can be seen in Fig. 4. However, this disagreement would be solved if a younger population is present. We have therefore explored this possibility by assuming that the ionizing population is composed by two different bursts, one responsible for the WR emission and another that we have taken of 1.0 Myr that would provide the necessary excess of ionizing photons. The predicted values of WR EWs and fluxes for this composite population whose EW(Hβ) is that observed and corrected, are shown by solid thick lines in Fig. 3. It can be seen that no agreement is now found for the blue bump although the red bump values are well reproduced.

Part of this disagreement could be due to aperture effects. G00 point to a factor of 3.1 between the Hβ flux measured inside the slit and the total Hβ emission. If we assume that correction and consider the WR stars to be concentrated inside the slit, we obtain the fluxes and EW of the WR features shown in Fig. 5. The measured fluxes and EWs have been divided by the aperture correction factor, as a consequence of the increment of the emission of Hβ and its continuum and assuming it affects both quantities similarly. Again, we plot the same quantities corrected for the presence of the nebular continuum and the absorption of ionizing photons by dust. The predictions of the models are plotted with a solid thin line for a unique burst of star formation and a dashed line for continuous star formation. The solid thick line corresponds to a composite population with an instantaneous burst of the age showed along the *X*-axis, plus a population of 1.0 Myr, the two of them together providing the expected EW(Hβ). Now, we find agreement for both blue and red bump features in the high mass-loss rate case assuming either a constant star formation rate at an age of 3.6 Myr or a populations composed of a young cluster of 1.0 Myr and an older one with age 3.2 or 4.2 Myr which contains the WR stars. In the case of the continuous star formation rate, the agreement occurs for an age slightly higher than that compatible for the expected EW(Hβ), but probably within the errors.

We can calculate the mass of ionizing clusters in each case, using the number of ionizing photons, which can be obtained from the flux of Hα, from the relation:

$$\log Q(\mathrm{H}) = 11.86 + \log L(\mathrm{H}\alpha)$$

Taking into account the fraction, *f*, of photons absorbed by dust, the resulting number of ionizing photons is $10^{51.99\pm0.13}$. Neglecting the contribution to the number of ionizing photons by the underlying population:

$$Q(\mathrm{H}) = M_{\mathrm{yc}}\, Q(\mathrm{H})_{\mathrm{yc}} + M_{\mathrm{WR}}\, Q(\mathrm{H})_{\mathrm{WR}},$$

where M_{yc} and M_{WR} are the masses of the clusters of 1.0 Myr and in the WR phase, respectively, and $Q(\mathrm{H}\ \alpha)_{\mathrm{yc}}$ and $Q(\mathrm{H}\ \alpha)_{\mathrm{WR}}$, their corresponding numbers of hydrogen ionizing photons per unit mass. The relative contributions of each of the clusters to the total ionizing mass can be derived from the observed EW of Hβ using the equation below:

$$\frac{\mathrm{EW}(\mathrm{H}\beta)_{\mathrm{obs}} - \mathrm{EW}(\mathrm{H}\beta)_{\mathrm{yc}}}{\mathrm{EW}(\mathrm{H}\beta)_{\mathrm{WR}} - \mathrm{EW}(\mathrm{H}\beta)_{\mathrm{obs}}} = \frac{L_C(\mathrm{H}\beta)_{\mathrm{WR}}}{L_C(\mathrm{H}\beta)_{\mathrm{yc}}}$$

$$= \frac{L_C(\mathrm{H}\beta)_{\mathrm{WR}}/m}{L_C(\mathrm{H}\beta)_{\mathrm{yc}}/m}\,\frac{M_{\mathrm{WR}}}{M_{\mathrm{yc}}},$$

where $\mathrm{EW}(\mathrm{H}\beta)_{\mathrm{obs}}$ stands for the observed value of the EW of Hβ, $\mathrm{EW}(\mathrm{H}\beta)_{\mathrm{yc}}$, $\mathrm{EW}(\mathrm{H}\beta)_{\mathrm{WR}}$ are the predicted EWs for each of the clusters and $L_C(\mathrm{H}\beta)_{\mathrm{yc}}$ m^{-1}, $L_C(\mathrm{H}\beta)_{\mathrm{WR}}$ m^{-1} are the model predicted continuum luminosities per unit mass at the Hβ wavelength for each of the clusters.

The characteristics of the model ionizing clusters are listed in Table 4. The luminosities for the single ionizing clusters are given $M_{\odot}^{-1}$. Using these values and the expressions above, it is possible to calculate the cluster masses for each assumed case. For the composite population with clusters 1- and 3.2-Myr old, masses of 8.7×10^4 and 2.4×10^4 M$_{\odot}$ are found. For the 1- and 4.2-Myr-old clusters, the corresponding values are 9.3×10^4 and 3.3×10^4 M$_{\odot}$. This gives a total mass for the ionizing population of 1.11×10^5 and 1.26×10^5 M$_{\odot}$, respectively. In both cases the younger cluster makes up more than 70 per cent of this total mass and dominates the ionization providing more than 80 per cent of the hydrogen ionizing photons and about twice the continuum luminosity at Hβ than the cluster containing most of the WR stars. The observed luminosities of the blue and red bumps are better reproduced by the combination with

[1] We consider the contribution of the underlying stellar population in this knot which shows a very high value of EW(Hβ), to be negligible.

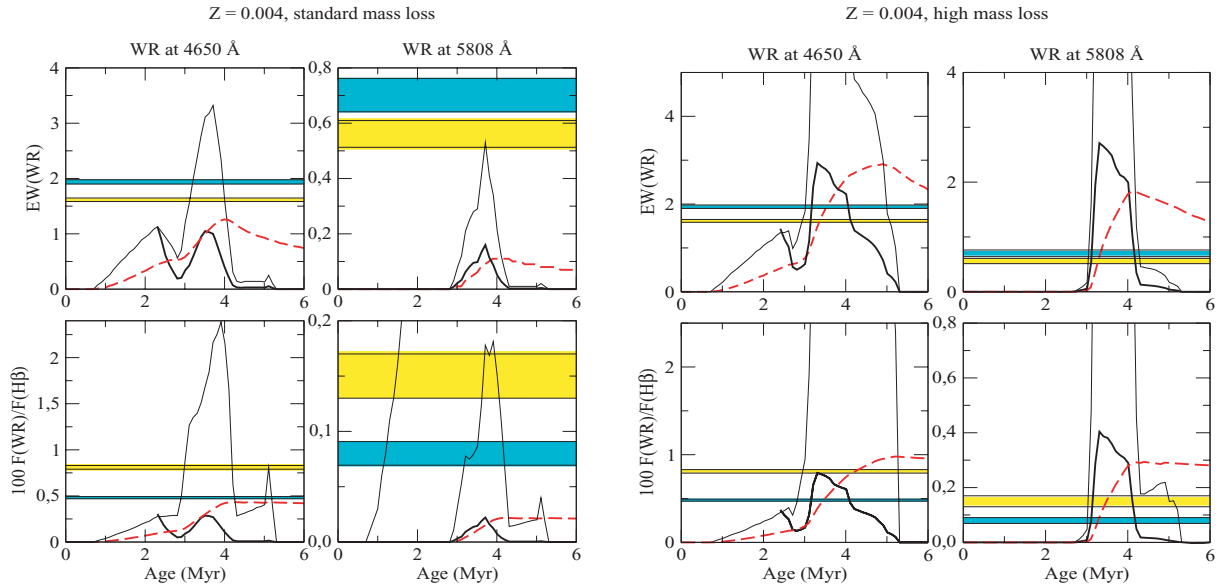

Figure 5. Comparison between the intensities and EWs of the WR red and blue bumps observed and aperture corrected in Mrk 209 and those predicted by the models. In the left-hand panels, models with standard mass-loss and in the right-hand panels, with high mass-loss. Both models have been calculated for a metallicity $Z = 0.004$. The bands stand for the same quantities represented in Fig. 3, but now taking into account the aperture correction. Models for an instantaneous burst are plotted as a solid thin black line. The solid thick line represent models of a composite population with an instantaneous burst with an age of 1 Myr, resulting in the expected EW(Hβ) in the slit (443 Å) and that assuming the aperture correction only for the 1.0-Myr population (514 Å).

Table 4. Characteristics of the ionizing clusters as derived using the calculated number of ionizing photons and EW of Hβ.

	Young cluster $M_\odot^{-1}$	WR cluster $M_\odot^{-1}$		Composite population		Continuous SF $M_\odot^{-1}$	Observed (corrected)
Age (Myr)	1	3.2	4.2	1, 3.2	1, 4.2	3.6	
log L(Hβ)[a]	34.62	34.47	34.16	39.64	39.61	33.85	39.63 ± 0.13
log L(WR, 4650)[a]	31.27	33.07	32.70	37.46	37.22	31.60	37.57 ± 0.13
log L(WR, 5808)[a]	–	32.71	31.81	36.57	36.32	31.11	36.74 ± 0.16
EW(Hβ) (Å)	555	220	167	443	443	427	443
EW(4650) (Å)	0.22	2.19	4.84	2.40	1.40	2.03	1.94 ± 0.04
EW(5808) (Å)	–	7.63	1.19	0.72	0.13	1.23	0.70 ± 0.06

[a]In units of erg s^{-1}.

the younger WR cluster, as well as the EWs of the WR features. On the other hand, a larger cluster mass value is found for the continuous star formation scenario: 6.0×10^5 M$_\odot$ with the masses derived from the WR blue and red luminosities being barely consistent with observations.

The found ranges for the mass of the starburst lie in a regime where stochastic fluctuations of the number of WR stars in relation to the expected value can still be important. In fact, the dispersion calculated by Monte Carlo simulations (Cerviño et al. 2002) for the total mass of the clusters reach 0.01 in F(WR)/F(Hβ) and 1 Å in the EW(WR) for both the blue and red bumps. This can affect the expected age of the cluster in the WR phase, but the condition of fitting at same time the EW of Hβ constrains the possible age to only 1 Myr around the obtained value. Nevertheless, we do not find serious discrepancies between the predictions by both scenarios, a composite population and a continuous star formation, about the number of WR stars, which is found to be approximately 4 or 5 WC stars and 1 WN star, and those obtained from comparing the blue and red bump luminosities, with the average luminosities of WC and WN stars.

4.3 Line temperatures, ionic abundances and ionization correction factors

The best-fitting model for the emission lines have been obtained by varying the properties of the geometry and the metal content of the gas for the obtained stellar energy distribution. Here we summarize for each ionic species the values of electron temperature and ionic abundances predicted by this model. In Fig. 6 we represent the radial profiles of the abundances of each ionic species in the best-fitting model along with the electron temperatures in order to illustrate the most representative temperature in the zones where each ionic species stays.

In order to calculate averages of the electron temperature, ionic fractions and ionization correction factors, we have considered volumetric integrations which fit better the observed values for models with a spherical geometry (Luridiana et al. 2002)

$$\left(\frac{X^i}{X}\right) \equiv \frac{\int_0^{R_S} N(X^i) N_\mathrm{e}\, \mathrm{d}R}{\int_0^{R_S} N(Xi) N_\mathrm{e}\, \mathrm{d}R}.$$

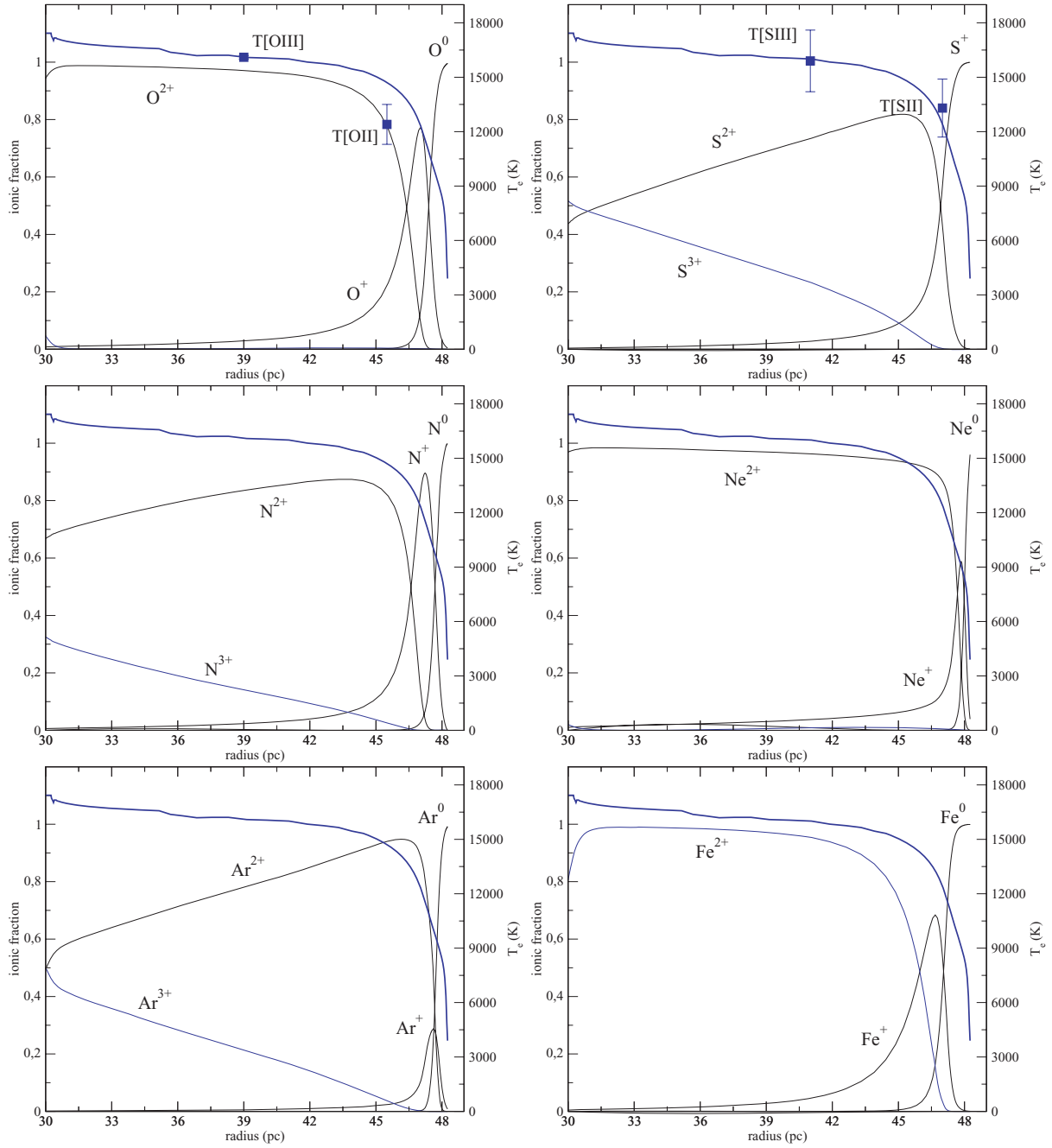

Figure 6. Radial profiles of the relative abundances of the most representative ionic species: oxygen, sulphur, nitrogen, neon, argon and iron. The radius indicates the distance to the ionizing cluster, with the ionization front located at 30 pc. The ionic fractions are marked on the left-hand side *y*-axes. The radial profile of the electron temperature is plotted for all the species along with their available measured values, which have been located at a distance that is a weighted average of the ionic fraction of the corresponding element. Its scale is marked on the right-hand side *y*-axes in all the plots.

The values obtained by the best-fitting model, along with the values obtained from the observations are tabulated in Table 5.

Oxygen: Both [O II] and [O III] electron temperatures are relatively well reproduced by the model. While T([O III]) results 2 per cent lower than the measured value, T([O II]) is overestimated by about 10 per cent. However, the lines involved in the determination of this temperature are widely separated and the measured error, mostly due to uncertainties in the reddening correction, is large. Using the measured [O III] temperature and the grid of models from PMD03, assuming the electron density obtained from [S II] lines, we would obtain a value for T([O II]) equal to 14 300 K leading to a value for $12 + \log(O^+/H^+)$ equal to 6.89 ± 0.11, which is more coincident with the result predicted by the model. Although the amount of O^+ is not especially relevant for the total abundance of oxygen for this object, due to its high degree of excitation, this amount becomes more important for the calculation of the ionization correction factors of some other species through the O^+/O quotient. The model gives as well a value of T([O III]) via the recombination lines allowing to estimate the fluctuations of temperature inside the

Table 5. Observed and model-predicted electron temperatures and ionic abundances.

	Measured	Model-predicted
T([O II]) (K)	12 400 ± 1100	13 930
$12 + \log(O^+/H^+)$	7.10 ± 0.11	6.88
T([O III]) (K)	16 200 ± 100	15 850
$12 + \log(O^{2+}/H^+)$	7.68 ± 0.01	7.74
$12 + \log(O/H)$	–	7.80
T([N II]) (K)	–	13 520
$12 + \log(N^+/H^+)$	5.64 ± 0.11	5.50
ICF(N^+)		9.38
$12 + \log(N/H)$	–	6.47
T([Ne III]) (K)	–	15 600
$12 + \log(Ne^{2+}/H^+)$	7.01 ± 0.01	6.98
ICF(Ne^{2+})		1.05
$12 + \log(Ne/H)$	–	7.00
T([S II]) (K)	13 300 ± 1600	13 270
$12 + \log(S^+/H^+)$	5.12 ± 0.11	5.05
T([S III]) (K)	15 900 ± 1700	15 600
$12 + \log(S^{2+}/H^+)$	5.86 ± 0.10	5.94
$12 + \log(S^{3+}/H^+)$	5.93 ± 0.20	5.52
$12 + \log(S^{3+}/H^+)^a$	5.68 ± 0.23	5.52
ICF(S^++S^{2+})		1.31
$12 + \log(S/H)$		6.11
T([Ar III]) (K)		15 350
$12 + \log(Ar^{2+}/H^+)$	5.31 ± 0.09	5.32
ICF(Ar^{2+})		1.22
T([Ar IV]) (K)		15 995
$12 + \log(Ar^{3+}/H^+)$	4.49 ± 0.05	4.59
ICF(Ar^{2+}+Ar^{3+})		1.02
$12 + \log(Ar/H)$		5.40
T([Fe III]) (K)		14 450
$12 + \log(Fe^{2+}/H^+)$	4.92 ± 0.22	5.01
ICF(Fe^{2+})		7.59
$12 + \log(Fe/H)$		5.89

[a]Assuming a constant S^{3+}/S^{2+} ratio. See text for details.

nebula, which could occasionally lead to an underestimate of the chemical abundance (Peimbert 1967). The value of 16 100 K for this temperature leads to a $t^2 = 0.004$, which is consistent with the measurements for BCD galaxies made using the temperature of the Balmer jump (Guseva, Izotov & Thuan 2006; Hägele et al. 2006), which point to values of t^2 negligible in these kind of objects. The total oxygen abundance is calculated under the assumption that the fractions of neutral hydrogen and oxygen are equal:

$$\frac{O^0}{O} = \frac{H^0}{H}$$

due to the charge-exchange reaction $O^+ + H^0 \rightarrow O^0 + H^+$ (see Osterbrock 1989), and this allows us to calculate O/H as

$$\frac{O}{H} = \frac{O^+ + O^{2+}}{H^+}.$$

In our model the neutral fraction of both elements are almost coincident: 0.021 for H^0/H and 0.019 for O^0/O.

Nitrogen: T([N II]) can be determined directly when the auroral line, at 5755 Å is measured. Nevertheless, in most objects, as in the case of Mrk 209, this line is not detected with enough signal-to-noise ratio. Therefore, the ionic abundance of N^+ is calculated under the assumption that T([N II]) ≈ T([O II]), since both ions lie in the low-excitation zone of the nebula. In our model, the electron temperature associated to the zone of N^+ is slightly lower than that of O^+ and, in fact, is closer to the value of T([S II]). The N^+/H^+ ionic abundance calculated with T([O II]) as derived from the measured T([O III]) using the grid by PMD03 is $12 + \log(N^+/H^+) = 5.51 \pm 0.02$, almost identical to the value predicted by our model.

The total abundance of nitrogen is calculated under the assumption that

$$\frac{N^+}{N} = \frac{O^+}{O}.$$

For our model, this approximation yields an ionisation correction factor of ICF(N^+) equal to 8.24, confirming the results predicted by the models in PMD03. The predicted value is slightly higher than the value obtained for the *hot* model from Mathis & Rosa (1991), which predicts ICF(N^+) = 6.44.

Neon: The ionic abundance of Ne^{2+} is calculated assuming that T([Ne III]) ≈ T([O III]), what seems well justified in view of the results of our model. The total abundance of neon is calculated assuming that

$$\frac{Ne^{2+}}{Ne} = \frac{O^{2+}}{O}$$

which, for our model yields, respectively, 0.95 and 0.85. This difference could be caused by the growing importance of the charge transfer between O^{2+} and H^0. According to Izotov et al. (2004) this effect is only noticeable when O^{2+}/O^+ is larger than 8. For this model, this quotient is 7.24, and the relative fraction of Ne^{2+} is slightly larger. On the other hand, the ICF(Ne^{2+}) from Mathis & Rosa (1991) is equal to 0.87.

Sulphur: For this element, there are two observable stages in the optical and the near-IR parts of the spectrum, respectively. For S^+, it is usual to assume that T([S II]) ≈ T([O II]), but in this object it is possible to measure the auroral lines of [S II] at 4068, 4076 Å. The derived [S II] line temperature is consistent with that of T([O II]) within the errors, which are large, and closer to the value predicted by the model. Thus, the derived and model calculated abundance of S^+ are similar. Regarding S^{2+}, the line temperature agrees rather well with the value predicted by the model and therefore the predicted ionic abundance is within the errors of the measured value. Both derived and predicted [S III] electron temperatures agree with the value obtained from T([O III]) using the empirical relation derived by Hägele et al. (2006), that is,

$$T([S\,III]) = (1.19 \pm 0.08)T([O\,III]) - (0.32 \pm 0.10).$$

The ionization correction factor of sulphur accounts for the fraction of S^{3+} in the inner parts of the nebula. The first assumption to calculate it was (Peimbert & Costero 1969):

$$\frac{S^+ + S^{2+}}{S} = \frac{O^+}{O}$$

but several authors have pointed that this approximation could overestimate the fraction of S^{+3} in high-excitation nebula. Thus, Barker (1980), proposed a new ICF for S^+ and S^{2+}:

$$\mathrm{ICF}(S^+ + S^{2+}) = \left[1 - \left(1 - \frac{O^+}{O}\right)^{\alpha}\right]^{-1/\alpha}$$

whose fit for the models by Stasińska (1978) gives a value of $\alpha = 3$. Later models (Stasińska 1990) have produced a lower value of $\alpha = 2$.

On the other side mid-IR observations for this object exist (Nollenberg et al. 2002) and allow us to measure directly the S^{3+} abundance and calculate the ICF($S^+ + S^{2+}$). The value found by Pérez-Montero et al. (2006) is 1.97 ± 0.62, which corresponds to Barker's formula for a value of $\alpha = 1.66$. In that same work, a new value of the S^{3+} abundance is proposed assuming a constant ratio of S^{3+}/S^{2+}, comparing the S^{2+} abundances in the near-IR (9069.9532 Å) and the mid-IR (18.71 μm). For our model, the predicted ICF($S^+ + S^{2+}$) is 1.31, slightly higher than the value obtained in PMD03 (1.22) but within the errors of the new calculated value by Pérez-Montero et al. (2006) which is 1.56 ± 0.76. The ICF predicted by our model corresponds to a value of $\alpha = 2.8$, slightly higher than the $\alpha = 2.5$ found in Pérez-Montero et al. (2006). The value obtained from Mathis & Rosa (1991) for this ICF is 2.28.

Argon: Only the emission lines of [Ar III] at 7137 Å and of [Ar IV] at 4713, 4740 Å are detected, thus allowing to calculate the ionic abundances of Ar^{2+} and Ar^{3+}, respectively. The assumptions T([Ar III]) ≈ T([S III]) and T([Ar IV]) ≈ T([O III]) are well justified in both cases.

Since Ar^{3+} is not usually detected in spectra, the ionization correction factor for argon refers to Ar^{2+}. The ICF(Ar^{2+}) expression in Izotov, Thuan & Lipovetsky (1994) from the models of Stasińska (1990) yields a value of 2.51, while in our model a value of 1.32 is found. Using the coefficients from Mathis & Rosa (1991), the ICF is found to be 21.6. Martín-Hernández et al. (2002) have proposed the relation: $N^{2+}/N^{+} \approx Ar^{2+}/Ar^{+}$. The result of our model for the first quotient is 7.21, while for the second one it is 41.98, what is far away from the expected result.

Iron: The only visible species in the optical spectrum of this galaxy is Fe^{2+} through the 4658 Å line. For this stage of iron ITL97 propose T([Fe III]) ≈ T([O II]). In our model the agreement between both temperatures is good, although the line temperature of Fe^{2+} is slightly higher.

The ICF proposed by ITL97 from Stasińska's (1990) models is

$$\frac{\mathrm{Fe}}{\mathrm{Fe}^{2+}} = 1.25\frac{\mathrm{O}}{\mathrm{O}^{+}}$$

which results in an ICF(Fe^{2+}) = 10.30, slightly higher than the value predicted by our model, equal to 7.59, and the value obtained using the ICF scheme proposed by Rodríguez & Rubin (2004):

$$\mathrm{ICF}(\mathrm{Fe}^{2+}) = \left[\frac{\mathrm{O}^{+}}{\mathrm{O}^{2+}}\right]^{0.09}\frac{\mathrm{O}}{\mathrm{O}^{+}}$$

which gives in our model a value of 6.90.

5 SUMMARY AND CONCLUSIONS

We present a self-consistent model for the brightest knot of the BCD galaxy Markarian 209 calculated using the photoionization code CLOUDY 96. In order to fit the more relevant emission lines emitted by the ionized gas, we have introduced as input parameters some of the observed and deduced properties of this object, including radius, metallicity, WR features, the Hα flux and the relative fluxes of the more relevant emission lines observed both in the optical and near-IR. The addition to the analysis of the far-red emission lines, including [O II]λ7319, 7330 Å and [S III] 9069, 9532 Å, allows us to derive with more confidence the ionic abundances of oxygen and sulphur, as well as the ionization parameter and the equivalent effective temperature, by means of the [S II]/[S III] ratio (Díaz et al. 1991) and the η parameter (Vílchez & Pagel 1988), respectively.

Our model uses as input the spectral energy distribution produced by newly formed stellar clusters which has been calculated using evolutionary synthesis techniques (Leitherer et al. 1999) and the models atmospheres from Pauldrach et al. (2001) and Hillier & Miller (1998). A metallicity of $1/20\,Z_{\odot}$ ($Z = 0.004$), as corresponding to the O/H abundance derived for this object, has been adopted. The ionization front is located at a distance of 30 pc from the ionizing cluster and the thickness of the ionized region is approximately 18 pc. The total radius is close to that measured on Hα images. The model assumes a constant density of 190 cm^{-3}, as obtained from nebular diagnostics.

The addition of a certain amount of dust was required in order to reproduce correctly the measured electron temperatures. This dust implies a gas/dust ratio of 6.13×10^{-3}, identical to that in the Milky Way, and a fraction of absorbed photons of 0.58. The dust is included in the CLOUDY model using the command PGRAINS which provides a more realistic treatment of the physics of the dust in the nebula. The model-predicted reddening allows us to correct the measured $B - R$ index in the region of the burst to a value in agreement with the predicted colour index for the stellar ionizing populations used in the model. Nevertheless, the logarithmic extinction at Hβ predicted by the model for the included amount of dust, C (Hβ) = 0.19, is not compatible with the value deduced from the Balmer decrement (C (Hβ) = 0.06). This could be caused by an irregular distribution of the dust into the gas.

We have used the flux of Hα, the EW of Hβ and the fluxes and EWs of the WR features in order to constrain the age and properties of the ionizing cluster. Agreement between measured and predicted quantities is found for a composite population of two clusters, one very young, with an arbitrary age of 1.0 Myr, and another one in the WR phase with either 3.2 or 4.2 Myr. A marginal agreement is also found for an extended burst of star formation with 3.6 Myr. This scenario of continuous star formation is compatible with the results found by Terlevich et al. (2004) from the distribution of EW(Hβ) in H II galaxies. The masses deduced for the clusters lay in a range where the effect of stochastic effects in the number of massive stars can cause variations in the predicted quantities but not affecting the main conclusions of our work.

We have compared measured and model predicted electron temperatures. The presence of the dust allows us to reproduce the auroral lines of [O III] and [S III] and therefore the electron temperatures for these species, without appealing to any other mechanism of heating in the high-excitation zones of the ionized gas. Regarding the electron temperatures in the low-excitation zone, the temperature of [S II] is well reproduced, while for [O II], is slightly overestimated by the model, although it should be bore in mind that its determination carries large observational errors. This could affect the derived O^{+} ionic abundance although it should not affect the total derived abundance of oxygen, since most of it appears as O^{2+}. The electron temperatures for the rest of the ionic species follow the usual assumptions about the inner structure of the nebula and the determination of their chemical abundances are predicted to be within the errors of the measured quantities in most cases. The model predicts no fluctuations of temperature in agreement with results found in blue compact galaxies from measurements of the Balmer jump (Guseva et al. 2006; Hägele et al. 2006).

Using the ionization correction factors predicted by the models for the various species, we can calculate their total chemical abundances and therefore we can refine the derivation of some relevant abundance ratios. For N/O, we obtain −1.33, in agreement with the values expected for a certain amount of nitrogen produced as secondary. For S/O, the model predicts a value of −1.69, consistent with the constant value found for the sample of H II galaxies with measurements of the [S III] lines at 9069, 9532 Å and which is

slightly lower than the value measured for the Sun (Pérez-Montero et al. 2006). This is also the case for Ne/O and Ar/O for which values of −0.8 and −2.34, respectively, are found.

ACKNOWLEDGMENTS

We would like to thank M. Castellanos, C. Esteban, E. Pérez, E. Terlevich and J. M. Ví lchez for very interesting discussions and suggestions, R. Garcí a-Benito for his help with the photometric images and the referee, Daniel Kunth, for many valuable suggestions and comments, which have helped us to improve this paper.

This work has been supported by project AYA-2004-08260-C03-03 of the Spanish National Plan for Astronomy and Astrophysics. Also, partial support from the Comunidad de Madrid under grant S0505/ESP/000237 (ASTROCAM) is acknowledged. ÁID acknowledges support from the Spanish MEC through a sabbatical grant PR2006-0049 and thanks the hospitality of the Institute of Astronomy of Cambridge where the final version of this paper was written.

REFERENCES

Aloisi A., Leitherer C., 2000, A&AS, 197, 3001
Barker T., 1980, ApJ, 240, 99
Cerviño M., Valls-Gabaud D., Luridiana V., Mas-Hesse J. M., 2002, A&A, 381, 51
Conti P. S., 1991, ApJ, 377, 115
Deharveng J.-M. et al., 1994, A&A, 288, 413
De Robertis M. M., Dufour R. J., Hunt R. W., 1987, J. Royal Astron. Soc. Canada, 81, 195
Díaz Á.I., Terlevich E., Vílchez J. M., Pagel B. E. J., Edmunds M. G., 1991, MNRAS, 253, 245
Fanelli M. N., O'Connell R. W., Thuan T. X., 1988, ApJ, 334, 665
Ferland G. J., Korista K. T., Verner D. A., Ferguson J. W., Kingdon J. B., Verner E. M., 1998, PASP, 110, 761
Garnett D. R., 1989, ApJ, 345, 282
Garnett D. R., 1992, AJ, 103, 1330
Gil de Paz A., Madore B. F., Pevunova O., 2003, ApJS, 147, 29 (GMP03)
González Delgado R. M., Pérez E., 2000, MNRAS, 317, 64
Guseva N. G., Izotov Y. I., Thuan T. X., 2000, ApJ, 531, 776 (G00)
Guseva N. G., Izotov Y. I., Thuan T. X., 2006, ApJ, 644, 890
Hägele G. F., Pérez-Montero E., Díaz Á. I., Terlevich R., Terlevich E., 2006, MNRAS, 372, 293
Hillier D. J., Miller D. L., 1998, ApJ, 496, 407
Izotov Y. I., Thuan T. X., Lipovetsky V. A., 1994, ApJ, 435, 647
Izotov Y. L., Thuan T. X., Lipovetsky V. A., 1997, ApJS, 108, 11 (ITL97)
Izotov Y. L., Stasińska G., Guseva N. G., Thuan T. X., 2004, A&A, 415, 87
Kunth D., Östlin G., 2000, A&AR, 10, 1
Lanz T., Hubeny I., 2003, ApJS, 147, 225
Leitherer C. et al., 1999, ApJS, 123, 3
Loose H. H., Thuan T. X., 1986, Star Forming Dwarf Galaxies and Related Objects. Editions Frontières, Les Ulis, p. 73
Luridiana V., Esteban C., Peimbert M., Peimbert A., 2002, Rev. Mexicana Astron. Astrofisica, 38, 97
Martín-Hernández N. L. et al., 2002, A&A, 381, 606
Mas-Hesse J. M., Kunth D., 1999, A&A, 349, 765
Mathis J. S., Rosa M. R., 1991, A&A, 245, 625
Mathis J. S., Rumpl W., Nordsieck K. H., 1977, ApJ, 217, 425 (MRN)
Noeske K. G., Papaderos P., Cairós L. M., Fricke K. J., 2005, A&A, 429, 115
Nollemberg J. G., Garnett D. R., Dinerstein H. L., 2002, ApJ, 581, 1002
Osterbrock D. E., 1989, Astrophysics of Gaseous Nebulae and Active Galactic Nuclei. Freeman & Co., San Francisco
Papaderos P., Loose H.-H., Thuan T. X., Fricke K. J., 1996, A&AS, 314, 59
Pauldrach A. W. A., Hoffmann T. L., Lennon M., 2001, A&A, 375, 161
Peimbert M., 1967, ApJ, 150, 825
Peimbert M., Costero R., 1969, Boletin Obs. Tonantzintla Tacubaya, 5, 3
Pérez-Montero E., Díaz Á.I., 2003, MNRAS, 346, 105 (PMD03)
Pérez-Montero E., Díaz Á. I., Vílchez J. M., Kehrig C., 2006, A&A, 449, 193
Pradham A. K., 1976, MNRAS, 177, 31
Raimann D., Bica E., Storchi-Bergmann T., Melnick J., Schmitt H., 2000, MNRAS, 314, 295
Rodríguez M., Rubin R. H., 2004, IAU Symp., 217, 188
Sargent W. L. W., Searle L., 1970, AJ, 162, L155
Schaerer D., Contini T., Pindao M., 1999, A&AS, 136, 35
Schulte-Ladbeck R. E., Crone M. M., Hopp U., 1998, ApJ, 493, 23
Schulte-Ladbeck R. E., Hopp U., Greggio L., Crone M. M., Drozdovsky I. O., 2001, AJ, 121, 3007
Shaw R. A., Dufour R. J., 1995, Pub. Astron. Soc. Pac., 107, 896
Smith L. J., Norris R. P. F., Crowther P. A., 2002, MNRAS, 337, 1309
Spitzer L., 1978, Physical Processes of the Interstellar Medium. Wiley, New York
Stasińska G., 1978, A&A, 66, 257
Stasińska G., 1990, A&AS, 83, 501
Stasińska G., Izotov Y. I., 2003, A&A, 397, 71
Terlevich R., Sylich S., Rosa-González D., Terlevich E., 2004, MNRAS, 348, 1191
van Hoof P. A. M., Weingartner J. C., Martin P. G., Volk K., Ferland G. J., 2004, MNRAS, 350, 1330
Viallefond F., Thuan T. X., 1983, ApJ, 269, 444
Vílchez J. M., Pagel B. E. J., 1988, MNRAS, 231, 257
Wang W., Liu X.-W., Zhang Y., Barlow J., 2004, A&A, 427, 873
Wu Y., Charmandaris V., Hao L., Brandl B. R., Bernard-Salas J., Spoon H. W. W., Houck J. R., 2006, ApJ, 639, 157
Zeippen C. J., 1982, MNRAS, 198, 111

This paper has been typeset from a TEX/LATEX file prepared by the author.